Spatiotemporal control of ultrashort laser pulses using intense single-cycle terahertz pulses

Yuzhen Shen,[1] G. L. Carr,[1] James B. Murphy,[1] Thomas Y. Tsang,[2] Xijie Wang,[1] and Xi Yang[1]
[1]*National Synchrotron Light Source, Brookhaven National Laboratory, Upton, New York 11973, USA*
[2]*Instrumentation Division, Brookhaven National Laboratory, Upton, New York 11973, USA*
(Received 17 July 2008; published 10 October 2008)

We demonstrate that the intense electric field of a subpicosecond single-cycle terahertz pulse can control and manipulate the temporal, spectral, and spatial phase of a copropagating ultrashort laser pulse through the Pockels effect in an electro-optic crystal. In the temporal and spectral domains, the single-cycle THz pulse can impart either a positive or a negative quadratic phase modulation to the probe pulse, leading to a spectral shift, broadening, or pulse expansion or compression. While acting in the spatial domain, the THz-induced phase modulation induces a lenslike effect, providing focusing or defocusing of the copropagating probe beam. The experimental results are in good agreement with simulations. Our study gives a comprehensive picture of the nonlinear spatiotemporal dynamics in the high-field regime driven by the intense single-cycle THz pulse.

DOI: 10.1103/PhysRevA.78.043813 PACS number(s): 42.65.Sf, 42.65.Re

I. INTRODUCTION

When an intense optical pulse propagates through a nonlinear medium it causes a change of the refractive index, which in turn induces a phase shift. The associated optical phenomenon is referred to as the Kerr or Pockels effect, depending on the order of the nonlinear effect. The Kerr effect in the temporal domain results in self-phase-modulation (SPM); but it can also occur in the spatial domain, where it produces self-focusing or self-defocusing, which is known as Kerr lensing [1–3]. When a weak probe pulse co-propagates with the intense pulse through the nonlinear medium, the probe pulse undergoes a phase modulation due to the temporal and spatial variation of the nonlinear index of refraction originating from the intense primary pulse, leading to a substantial modification of the temporal, spectral, and spatial profile of the probe pulse. Such a process is defined as cross-phase modulation (XPM), and has been extensively studied via the third-order Kerr effect [1,2]. The same concepts apply to the second-order Pockels effect, except that now the induced index change is driven by the electric field instead of the intensity. When the Pockels effect is used for XPM, the incident light pulse usually experiences periodic sinusoidal phase modulation, which generates sidebands at frequencies that are the sum and difference of the carrier frequency of the incident light and integer multiples of the modulating frequency of the applied electric field. The amplitude of each pair of sidebands is given by Bessel functions [3]. However, this may not be the case if the applied field is far from sinusoidal and contains few or only one field cycle. Such a study is essentially unexplored and thus represents a novel and interesting subject for ultrafast science. In recent years, with advances in ultrafast technology, it is possible to generate intense single-cycle and near-single-cycle electromagnetic pulses of subpicosecond temporal duration by a variety of methods and sources [4–9]. These pulses have center frequencies in the terahertz range, and consist of one electric field oscillation under the pulse envelope. Their peak electric field is very high, and varies rapidly from one half cycle to the next, which can be used as an ultrafast electric-field pulse. In this work, we demonstrate that an intense single-cycle THz pulse induces nonlinear phase modulation in an electro-optic crystal via its strong electric field through the Pockels effect. The time-dependent phase modulation is used to manipulate the temporal, spectral, and spatial characteristics of a weak copropagating laser probe pulse that is short compared to the time variation of the THz pulse. By adjusting the time delay of the probe pulse to coincide with different portions of the single-cycle THz pulse, the probe pulse can develop either positive or negative temporal, spectral, and spatial phase modulation. In the spectral domain, it leads to spectral broadening with either a positive or negative frequency chirp; in the temporal domain, it leads to pulse expansion or compression when combined with group velocity dispersion (GVD); in the spatial domain, the result is focusing and breakup or defocusing. In analogy to Kerr lensing, we call this lensing effect "Pockels lensing." Our study also indicates that the intense single-cycle THz pulses open a new regime in ultrafast and nonlinear optics.

II. EXPERIMENTAL SETUP

The experiments were carried out by using the coherent THz source developed at the National Synchrotron Light Source of Brookhaven National Laboratory [7]. A schematic diagram is shown in Fig. 1(a). The THz pulses are generated using a subpicosecond relativistic electron bunch through coherent transition radiation. The electron bunches, containing on the order of 10^{10} electrons, are accelerated to $\sim$120 MeV and then compressed to less than $\sim$1 ps [full width at half maximum (FWHM)]. The transition radiation is produced by the interaction of the electron bunches with a metal target, which results in subpicosecond single-cycle THz radiation with spectral content up to $\sim$2 THz. The THz wave form is measured by a single-shot electro-optic (EO) sampling technique using a chirped laser pulse [10], and is shown in Fig. 1(b). A Ti:sapphire laser amplifier produces a transform-limited pulse of $\sim$120 fs (FWHM) at 795 nm, which is employed as a probe and is actively synchronized with the radio-frequency clock of the accelerator. The probe pulse copropagates with the THz pulse through a 1-mm-thick ZnTe crystal such that the electric-field vector of the THz is paral-

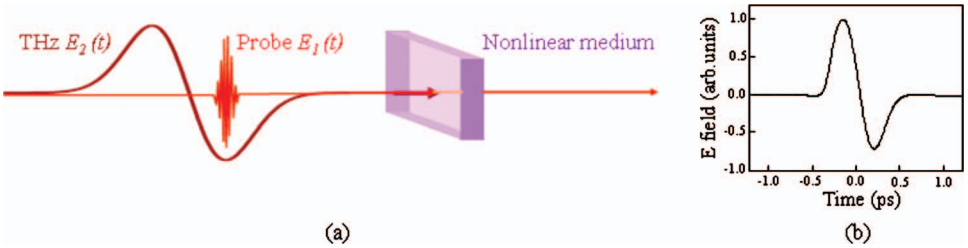

FIG. 1. (Color) (a) Schematic diagram of single-cycle THz-induced cross-phase modulation on a copropagating ultrashort laser pulse in a nonlinear medium. (b) Measured single-cycle THz wave form.

lel to the ZnTe [001] direction and the probe polarization perpendicular to the [001] direction [11]. The group delay dispersion induced by the ZnTe and the transport optics is compensated for by a grating compressor. The spot size at the EO crystal position is ~1 mm for the probe beam and ~2 mm for the THz. A wire mesh attenuator is used to limit the THz energy on the ZnTe crystal to ~35 μJ. The corresponding *E*-field strength at the ZnTe crystal is estimated to be $\sim 4\times 10^7$ V/m for which the refractive index change in ZnTe is dominated by the Pockels effect; the Kerr effect can be neglected [7,12]. Experiments are conducted to measure the spectrum, the spectrogram, and the spatial profile of the probe as a function of the time delay between the THz and the probe pulses, all recorded simultaneously for each pulse with a spectrometer, a second-harmonic generation (SHG) frequency-resolved optical gating (FROG) device, and a charge-coupled device (CCD) camera. The intrinsic direction-of-time ambiguity present in the retrieved pulse from the SHG FROG device was removed by an additional FROG measurement after chirping the probe pulse with a piece of glass of known group velocity dispersion.

III. TEMPORAL AND SPECTRAL CHARACTERISTICS

The temporal and spectral measurement results are shown in Fig. 2. The cartoon shown in column 1 of Fig. 2 illustrates that the probe pulse interacts with different parts of the single-cycle THz pulse by changing the time delay. The second column shows the measured FROG traces of the probe pulse for each time delay. The FROG trace is a three-dimensional graph, with time on the horizontal axis, frequency on the vertical axis, and intensity encoded as color. The reconstructed FROG traces are visually identical to the measured traces and are not shown. The retrieved pulses in the time and frequency domains, including intensity and phase, are shown in columns 3 and 4. The independently measured probe spectrum is plotted in column 5 for comparison, and it closely matches the retrieved spectra. The first row of Fig. 2 shows that the probe phase in the absence of THz is constant over the pulse duration and the spectrum, and hence represents a nearly transform-limited pulse. As the probe is scanned across the single-cycle THz *E* field, the spectrum is shifted toward the blue when the probe overlaps the central zero crossing of the THz *E* field, and toward red at the leading and trailing edges, as shown in the second, fourth, and sixth rows of Fig. 2. The wavelength shift is accompanied by a small asymmetric spectral broadening and the probe pulse is slightly chirped. The central wavelength of the probe is shifted as much as ~10 nm toward the blue side and ~6 nm toward the red.

The temporal variation of the THz *E* field not only leads to a wavelength shift but also introduces a spectral broadening of the probe pulse. By adjusting the time delay between the probe and the single-cycle THz pulses, the maximum

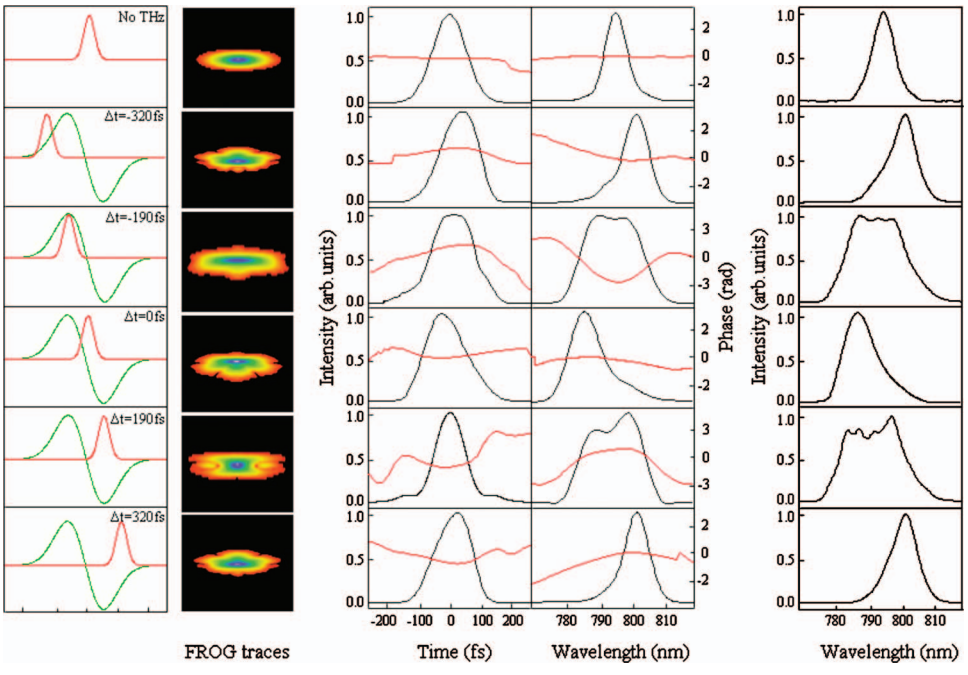

FIG. 2. (Color) Temporal and spectral effects of cross-phase modulation with an intense single-cycle terahertz pulse. Column 1, a cartoon illustrating that, with a change in the time delay, an ultrashort probe pulse (red) interacts with different parts of a single-cycle THz pulse (green). Column 2, measured SHG FROG traces as a function of time delay between the THz and probe pulses. Column 3 and 4, retrieved intensity (black) and phase (red) in time and frequency domains. Column 5, independently measured probe spectra.

spectral broadening takes place when the probe pulse overlaps with the crest or trough of the THz E field. The corresponding FROG traces can be seen in the third and fifth rows of Fig. 2. The spectral broadening is extended to over ~30 nm, and both the spectral and temporal phases are predominately parabolic, indicating that the THz E field imposed a nearly linear chirp across the probe pulse. Note that the spectral shapes of the probe at the crest and the trough are nearly identical, but the phase is reversed and the frequency chirp is changed from positive to negative. Therefore the probe phase can be tuned between positive and negative by changing the delay between the THz and probe pulses. Physically, this can be understood by the fact that if the probe pulse is short compared to a half cycle of the single-cycle THz pulse, when overlapped at the crest or trough, the phase modulation imparted on the probe is approximately quadratic and therefore the instantaneous frequency is nearly linearly chirped. Since the THz E field changes polarity from positive to negative, the sign of the phase modulation reverses. The spectral phases are fitted to a polynomial, and the resulting positive and negative quadratic phase coefficients are $\sim 7.5\times 10^3$ and $\sim -2.6\times 10^3$ fs^2, respectively. The probe pulse is slightly broader when it interacts with the crest. While at the trough, the pulse is ~30 fs shorter, and is accompanied by a pedestal on the leading and trailing edges.

Such a spectrally broadened pulse can be compressed by passage through a dispersive element with either positive or negative GVD, depending on the sign of the chirp that the probe pulse acquires. For example, by adjusting the delay of the probe pulse to coincide with the crest of the single-cycle THz pulse, the phase modulation imparts a positive chirp on the probe pulse that, in turn, can be compensated for using a grating or prism compressor. When overlapped with the trough, the probe pulse develops a negative chirp, which can simplify the compressor to a flat plate of material such as fused silica. Assuming all the chirps could be compensated, the 30 nm bandwidth could support a transform-limited pulse of ~30 fs duration.

Numerical modeling is performed for comparison with the temporal and spectral experiments. The copropagation of the THz and the probe laser in a nonlinear dispersive medium can be described by a set of coupled nonlinear Schrödinger equations [1],

$$\frac{\partial E_1}{\partial z}+\frac{1}{v_1}\frac{\partial E_1}{\partial t}+i\frac{\beta_1}{2}\frac{\partial^2 E_1}{\partial t^2}=i\kappa_1 E_2 E_1+i\gamma_1(2|E_2^2|+|E_1^2|)E_1, \tag{1}$$

$$\frac{\partial E_2}{\partial z}+\frac{1}{v_2}\frac{\partial E_2}{\partial t}+i\frac{\beta_2}{2}\frac{\partial^2 E_2}{\partial t^2}=i\kappa_2 E_1 E_2+i\gamma_2(2|E_1^2|+|E_2^2|)E_2, \tag{2}$$

where the indices 1,2 indicate the probe and THz pulses, respectively, E is the pulse envelope, β is the GVD coefficient, v is the group velocity, z is the coordinate along the propagation direction in the nonlinear medium, and κ and γ are the second-order Pockels and third-order Kerr coefficients, respectively. Note that there is a factor of 2 difference between the third-order XPM and SPM. Under our experimental conditions, the probe is weak so it does not affect itself (no SPM) or the strong THz pulse. Since the THz peak E field in our study is no more than 5×10^7 V/m, for ZnTe, $\kappa_1 E_2 \gg 2\gamma_1 E_2^2$. Therefore, the SPM term $|E_1^2|E_1$ and the third-order XPM term $2|E_2^2|E_1$ in Eq. (1) can be neglected.

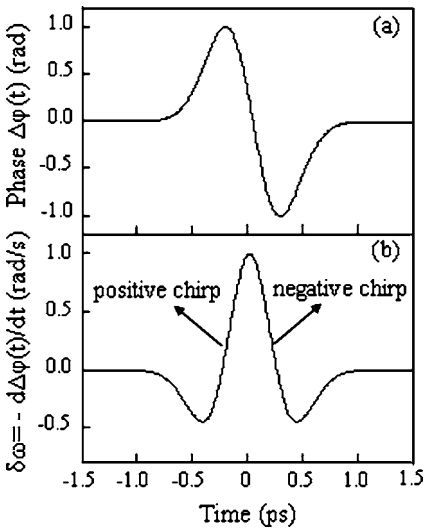

FIG. 3. Calculated phase shift and frequency shift versus time induced by a single-cycle THz pulse. (a) Normalized phase shift and (b) normalized frequency shift.

We first ignore GVD effects and explore the nonlinear phase shift $\Delta\varphi(t)$ induced by the single-cycle THz pulse on the probe through second-order XPM. In this approximation, an analytical solution can be found, given by $\Delta\varphi(t)=(2\pi\chi^{(2)}/n_0\lambda_1)\int_0^L E_2(t-\alpha z)dz$; where λ_1 is the central wavelength of the probe pulse, n_0 is the linear refractive index of ZnTe, L is the ZnTe thickness, $\chi^{(2)}$ is the second-order susceptibility, and the walk-off parameter $\alpha=1/v_1-1/v_2$ is calculated to be 150 fs/mm. The calculated phase shift [Fig. 3(a)] is proportional to the THz E field, although the walk-off leads to an overall reduction in the accumulated phase shift. The temporal variation of the induced frequency shift $\delta\omega$ [Fig. 3(b)] has several interesting features. First, when the probe interacts with different segments of the THz pulse, $\delta\omega$ is negative (redshifted) near the leading and trailing edges, and $\delta\omega$ is positive (blueshifted) at the zero crossing. Second, the probe acquires a positive chirp when scanned across the leading edge to the zero crossing of the THz pulse. The maximum spectral broadening occurs when the probe overlaps with the crest of THz pulse, and its frequency chirp is positive and linear. Third, the frequency chirp remains linear but reverses sign from positive to negative when the probe pulse is scanned from the zero crossing to the trailing edge. The second maximum of the spectral broadening occurs when probe coincides with the trough of the THz pulse, and the probe acquires a negative frequency chirp. This is consistent with the FROG measurements shown in Fig. 2.

We then numerically solved the nonlinear propagation equations by using a split-step Fourier method [1]. Figure 4 shows the simulation results of the spectral and temporal evolution of the probe pulse as it interacts with different portions of the single-cycle THz E field, in which the effects of both the GVD and XPM are taken into account. Note that

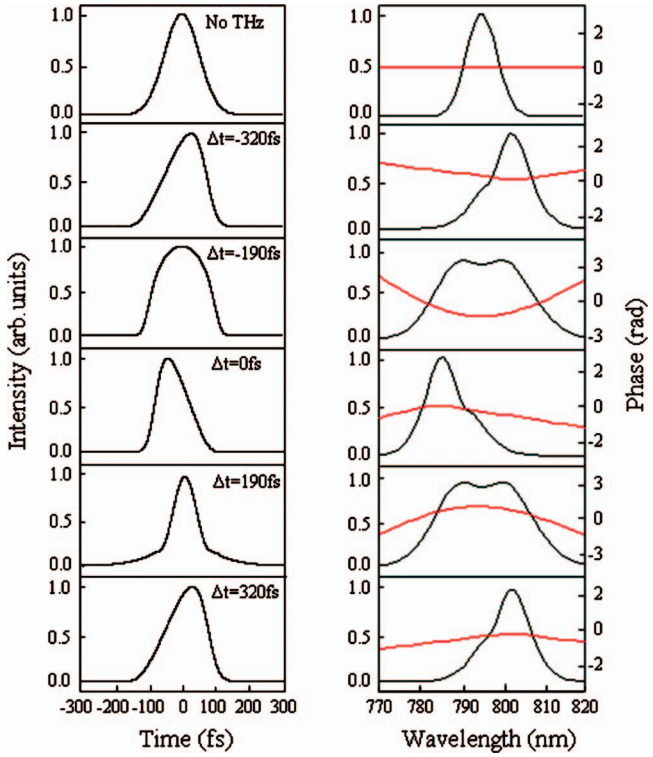

FIG. 4. (Color) Temporal and spectral shapes of the probe pulse as it is scanned across the single-cycle THz E field from numerical simulation. Spectral phase is shown by the red line.

the probe acquires a maximum quadratic phase but with opposite polarity when it is temporally overlapped with the crest or trough of the THz pulse. When the probe overlaps with the crest of THz E field, both the THz-induced XPM and ZnTe dispersion impose a positive chirp on the probe pulse. The interplay between the XPM and GVD increases the amount of spectral quadratic phase, leading to a broadening of the pulse, and leaves the pulse with a positive frequency chirp. The situation is different when the probe pulse overlaps with the trough of the THz E field, at which the XPM-induced frequency chirp is negative while the ZnTe dispersion-induced chirp is positive. The two chirp contributions can cancel each other along the center portion of the probe pulse, leading to a pulse shortening, and the probe pulse is left with a residual amount of negative quadratic phase. This is in agreement with the FROG measurements shown in Fig. 2.

IV. SPATIAL CHARACTERISTICS

The THz-induced phase modulation also affects the spatial profile of the probe laser. The intensity profiles of the probe laser are measured for different THz E-field strengths and for different time delays between the THz and the probe laser. The CCD camera is located ~15 cm away from the sample. Figure 5(a) shows the spatial profile of the probe laser when the THz is not present. When the time delay is varied such that the probe coincides with the crest of the THz, there is a clear contraction of the beam, indicating focusing. The beam size decreases with increasing THz E field, as shown in Figs. 5(b) and 5(c). With a further increase of the THz E-field strength, the probe beam breaks up into two spots and then collapses into a complex pattern with several hot spots, as illustrated in Figs. 5(d) and 5(e). However, when the probe overlaps with the trough of the THz pulse, the probe beam size is broadened and defocused, as shown in Fig. 5(f).

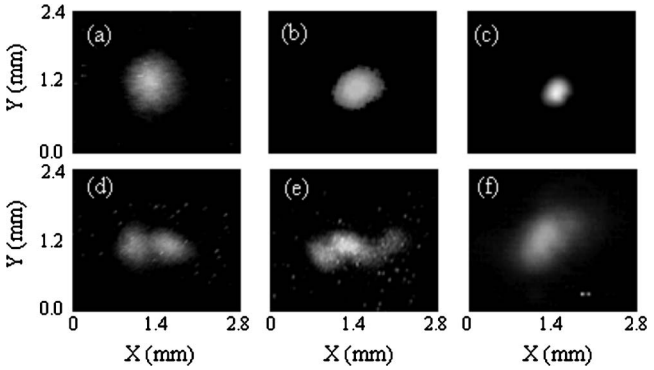

FIG. 5. Measured spatial profile of the probe beam. (a) Without THz, and E_{THz}=(b) 2.5×10^7, (c)=4.0×10^7 (d) 4.5×10^7 (e) 5.0×10^7, and (f) -4.0×10^7 V/m.

The physical origin of such a lensing effect can be understood by the fact that the distribution of the THz E field is both time and space dependent, and this leads to a phase modulation not only in time, but also in space [13]. Consider a THz pulse with a beam radius a propagating through ZnTe. If the THz E field's transverse profile is approximated by a parabola, the resulting phase shift is given by $\Delta\varphi(r,t)=[2\pi\chi^{(2)}E_{\mathrm{THz}}(t)L/n_0\lambda][1-(r/a)^2]$. This quadratic phase variation is equivalent to a lens of focal length $f=n_0a^2/2\chi^{(2)}E_{\mathrm{THz}}(t)L$. The focal length of the induced lens is controllable by changing the THz E-field strength and can be as short as ~35 cm with $E_{\mathrm{THz}}=4\times10^7$ V/m. As the probe copropagates with the single-cycle THz pulse through the ZnTe and coincides with the crest of the THz pulse, we have $E_{\mathrm{THz}}>0$, and therefore $\Delta\varphi(r,t)>0$. The THz pulse together with the EO crystal acts as a positive lens, imposing a converging wave front on the probe and thereby focusing it. If the time delay is adjusted to overlap the probe with the THz trough, then $E_{\mathrm{THz}}<0$ and $\Delta\varphi(r,t)<0$, and the induced positive lens switches to a negative lens. In analogy to Kerr lensing, we call this lensing effect Pockels lensing. It is different from the conventional Kerr lensing effect in that it is able to focus or defocus a light beam in the same nonlinear medium by simply switching the relative phase.

The beam breakup cannot be explained by the thin lens approximation, which is valid only if the THz-induced phase shift is small. For a large phase shift, this approximation breaks down. Under our experimental conditions, the effects of self-focusing of the probe itself and induced focusing by third-order Kerr effects can be neglected. Since the laser probe pulse width is much shorter than that of the THz pulse, the induced lensing effects occur on a time scale such that the change of the refractive index and phase shift do not evolve significantly. Therefore, the evolution of the probe and THz beams can be described by the following nonlinear coupled equations [1,2]:

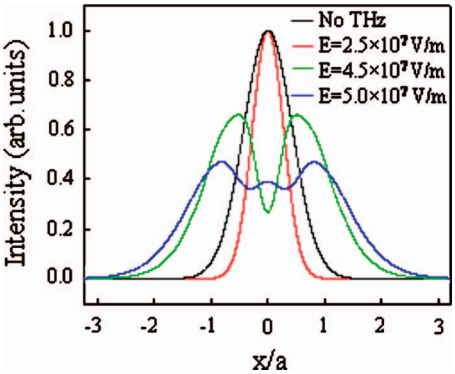

FIG. 6. (Color) Transverse probe beam profile with $E_{\mathrm{THz}}=0$ (black curve), 4.5×10^7 (green curve), and 5.0×10^7 V/m (blue) from numerical simulation.

$$\frac{\partial E_1}{\partial z} = i\frac{1}{2k_1}\frac{\partial^2 E_1}{\partial x^2} + i\kappa_1 E_2 E_1, \tag{3}$$

$$\frac{\partial E_2}{\partial z} = i\frac{1}{2k_2}\frac{\partial^2 E_2}{\partial x^2} + i\kappa_2 E_1 E_2, \tag{4}$$

where k is the wave vector, and the indices 1,2 indicate the probe and THz pulses, respectively. For simplicity we consider only one transverse coordinate x, and the initial probe and THz beams are assumed to be Gaussian in the transverse plane. Figure 6 shows the simulation result, which illustrates the beam breakup with increasing THz E-field strength.

V. CONCLUSIONS

In summary, we demonstrated that an intense single-cycle THz pulse can induce cross-phase modulation in an electro-optic crystal via its strong electric field through the Pockels effect. The temporal, spectral, and spatial effects of XPM on a weak laser probe pulse as it copropagates with the intense single-cycle THz pulse were investigated, and the experimental results are in good agreement with our numerical modeling. Our study gives comprehensive pictures of the nonlinear spatiotemporal dynamics in the high-field regime driven by an intense single-cycle THz pulse. The THz-induced XPM effect has important features that can be used to control and manipulate weak copropagating ultrashort optical pulses in the temporal and spatial domains. Our study also indicates that the single-cycle THz pulse with a high-peak E field offers unique opportunities for studying novel THz-induced nonlinear optical phenomena in the single-cycle regime.

ACKNOWLEDGMENTS

This work is supported by U.S. Department of Energy under Contract No. DE-AC02-98CH10886. The authors would like to thank Pooran Singh for technical support.

[1] G. P. Agrawal, *Nonlinear Fiber Optics*, 3rd ed. (Academic Press, London, 2001).
[2] R. Boyd, *Nonlinear Optics* (Academic, San Diego, CA, 2003).
[3] A. E. Siegman, *Lasers* (University Science Books, Mill Valley, CA, 1986).
[4] D. You, R. R. Jones, P. H. Bucksbaum, and D. R. Dykaar, Opt. Lett. **18**, 290 (1993).
[5] T. Bartel, P. Gaal, K. Reimann, M. Woerner, and T. Elsaesser, Opt. Lett. **30**, 2805 (2005).
[6] J. van Tilborg, C. B. Schroeder, C. Tóth, C. G. R. Geddes, E. Esarey, and W. P. Leemans, Opt. Lett. **32**, 313 (2007).
[7] Y. Shen, T. Watanabe, D. A. Arena, C.-C. Kao, J. B. Murphy, T. Y. Tsang, X. J. Wang, and G. L. Carr, Phys. Rev. Lett. **99**, 043901 (2007).
[8] F. Blanchard, L. Razzari, H. C. Bandulet, G. Sharma, R. Morandotti, J. C. Kieffer, T. Ozaki, M. Reid, H. F. Tiedje, H. K. Haugen, and F. A. Hegmann, Opt. Express **15**, 13212 (2007).
[9] J. Hebling, K.-L. Yeh, M. C. Hoffmann, B. Bartal, and K. A. Nelson, J. Opt. Soc. Am. B **25**, 6 (2008).
[10] Z. Jiang and X.-C. Zhang, Appl. Phys. Lett. **72**, 1945 (1998).
[11] S. Casalbuoni, H. Schlarb, B. Schmidt, P. Schmuser, B. Steffen, and A. Winter, TESLA Report No. 2005-01 (unpublished).
[12] J.-P. Caumes, L. Videau, C. Rouyer, and E. Freysz, Phys. Rev. Lett. **89**, 047401 (2002).
[13] A. Schneider, I. Biaggio, and P. Gunter, Appl. Phys. Lett. **84**, 2229 (2004).